Journal of Animal & Plant Sciences, 35(6): 2025, Page: 1720-1733
ISSN (print): 1018-7081; ISSN (online): 2309-8694
https://doi.org/10.36899/JAPS.2025.6.0146

ADOPTION OF PIEZOELECTRIC-ENHANCED POLYVINYL ALCOHOL/POLYVINYLIDENE FLUORIDE BILAYER COMPOSITE NANOHYDROGEL IN BONE AND CARTILAGE DEFECT REPAIR IN RABBITS

X. Sun[#], S. Wang[#], H.H. Tang, H.T. Yue and F. Ji*

Department of Orthopedics, The Affiliated Huai'an No.1 People's Hospital of Nanjing Medical University, Huai'an, 223300, Jiangsu, China.
#These authors contributed equally to this work.
*Corresponding author's Email: hayyjf@njmu.edu.cn

ABSTRACT

This study aimed to explore the therapeutic potential of piezoelectrically enhanced polyvinyl alcohol (PVA)/polyvinylidene fluoride (PVDF) bilayer composite nanohydrogel in bone and cartilage defect repair in rabbits. Employing silver nanowires (AgNWs) and nano-hydroxyapatite, a PVA/PVDF/AgNWs piezoelectric composite bilayer nanohydrogel was prepared and characterized through XRD, FTIR spectroscopy and electron microscopy. The piezoelectric, swelling, and mechanical properties of the nanohydrogel were evaluated. Rabbit bone marrow-derived mesenchymal stem cells (BMSCs) were divided into three groups: control, PVA/PVDF and PVA/PVDF/AgNWs groups. Cell viability was assessed via dual staining with acridine orange/propidium iodide (AM/PI) and visualized employing *ImageJ*. The expression of cartilage markers was measured by RT-PCR. A total of 30 rabbits with knee cartilage defects were divided into Group A (no intervention, blank control), Group B (intervention with PVA/PVDF hydrogel), and Group C (intervention with PVA/PVDF/AgNWs hydrogel), each with 10 rabbits. Gross observation and histological analysis were performed at eight weeks post-operation for cartilage repair evaluation.The PVA/PVDF/AgNWs piezoelectric composite bilayer nanohydrogel exhibited a three-dimensional network structure. The tensile fracture strength increased from 0.26 MPa to 0.6 MPa as the ethanol concentration increased. There was no significant difference in the proportion of live cells among the PVA/PVDF and PVA/PVDF/AgNWs groups and the control group (P>0.05). However, the expression levels of cartilage markers COL2A1, ACAN, and SOX9 were significantly higher in both experimental groups compared to the control group (P<0.05). In Group C, the defect site was almost completely covered by new cartilage, which showed significantly improved repair. Additionally, Group C exhibited significantly higher ICRS and histological scores than Groups A and B (P<0.05). The PVA/PVDF/AgNWs composite bilayer nanohydrogel exhibited low biotoxicity. It greatly enhanced chondrocyte growth and cartilage repair of rabbits, making it a valuable candidate in cartilage regeneration.

Keywords: polyvinyl alcohol; polyvinylidene fluoride; nanohydrogel; osteochondral defect; rabbit

This article is an open access article distributed under the terms and conditions of the Creative Commons Attribution (CC BY) license (https://creativecommons.org/licenses/by/4.0/)

Published first online October 29, 2025 Published final November 30, 2025

INTRODUCTION

Cartilage tissue repair has remained a clinical challenge in the field of medicine. Cartilage, a critical tissue in the human body, plays a pivotal role in maintaining normal joint function and supporting the entire skeletal system (Khajeh *et al*. 2021; Campos *et al*. 2019). Nevertheless, cartilage has very limited self-healing capacity. As a result, injuries or degeneration of cartilage typically lead to significant joint pain and impaired mobility. This issue is particularly evident in cases of trauma, osteoarthritis, and other related conditions, severely impacting the quality of life of affected individuals (Cooper and Rainbow 2022; Wang *et al*. 2023; SantAnna *et al*. 2022).

To address the challenges associated with cartilage injuries and degradation, hydrogel materials have garnered considerable attention as a therapeutic option. Due to their high water retention properties and excellent biocompatibility, hydrogels hold significant potential in the field of cartilage tissue repair (Zhang *et al*. 2021; Zhu *et al*. 2022). Nevertheless, conventional hydrogel materials are inherently passive and lack the capacity to stimulate surrounding cells, thereby limiting their effectiveness in promoting cartilage regeneration. Furthermore, the mechanical properties and stability of hydrogels present challenges, especially in long-term applications and within biological environments (Benmassaoud *et al*. 2020). Therefore, the development of a hydrogel material capable of actively promoting cell

activity through intrinsic mechanisms is essential for effective cartilage tissue repair. It is envisioned that such a hydrogel could enhance chondrocyte proliferation and differentiation, thereby accelerating cartilage regeneration and demonstrating excellent biocompatibility and mechanical performance (Abdollahiyan *et al*. 2020; Shen *et al*. 2022).

Polyvinyl alcohol (PVA) is a widely used hydrogel material in the medical field, highly favored by researchers due to its excellent biocompatibility and tunable physical properties (Zhao *et al*. 2020; Anastasio *et al*. 2024; Zhao *et al*. 2019; Li *et al*. 2019). In cartilage repair, the incorporation of the piezoelectric material polyvinylidene fluoride (PVDF) into PVA hydrogels offers significant potential, imparting unique functionalities to the PVA hydrogel material (Li *et al*. 2019). This functionality primarily arises from the piezoelectric effect exhibited by PVDF, which refers to its ability to generate charges and induce changes in electric potential when subjected to external mechanical pressure or strain (Bai *et al*. 2022; Torres-Rodriguez *et al*. 2022). Through interactions with cartilage cells, the piezoelectric effect of PVDF generates weak but continuous electrical stimulation. This electrical stimulation has been shown to positively influence cell proliferation and differentiation. In the context of cartilage repair, this stimulation can activate nearby cartilage cells, encouraging their more active involvement in tissue repair processes, thereby accelerating cartilage regeneration (Sakarkar *et al*. 2020; Vishwakarma *et al*. 2023). Furthermore, the piezoelectric properties of PVDF enable PVA/PVDF hydrogels to mimic mechanical stimulation in physiological environments. This is crucial for cartilage cells since they are typically subjected to mechanical stimuli originating from joint movements and bodily loads. By introducing this physiological mimicry into cartilage repair, PVA/PVDF hydrogels can better assist cartilage cells in achieving natural repair (Pour *et al*. 2020; Jabeen *et al.* 2024). To maximize the benefits of PVDF, PVA/PVDF hydrogels are designed with a bilayer structure. This configuration creates a distinct interface between PVA and PVDF, allowing for more efficient transmission of mechanical and electrical signals, thereby enhancing the piezoelectric effect of PVDF. This enhancement can improve the overall performance of PVA/PVDF hydrogels, making them more suitable for cartilage repair (Wang *et al*. 2022; Yu *et al*. 2021). Furthermore, the bilayer structure separates PVA and PVDF materials, avoiding mutual interference between them. This helps ensure that the piezoelectric properties of PVDF are fully utilized while maintaining the stability and biocompatibility of PVA hydrogels. Additionally, the bilayer structure allows for the modulation of material properties in different layers of PVA and PVDF (Ahmadi *et al*. 2019; Li *et al*. 2023).

The construction of a PVA/PVDF/silver nanowires (AgNWs) piezoelectric composite double-layer nano-hydrogel was prepared using AgNWs and nano-hydroxyapatite. Its quality was evaluated through characterization and performance analysis. Subsequently, *in vitro* cell and *in vivo* embedding experiments were conducted to investigate the application effectiveness of this hydrogel in cartilage tissue repair of rabbits. The aim was to provide an experimental basis and theoretical foundation for the development of innovative methodologies for cartilage defect treatment.

MATERIALS AND METHODS

Fabrication of PVA/PVDF/AgNWs piezoelectric composite double-layer hydrogel： (1) Preparation of PVA/PVDF hydrogel was as follows: 7.5 g of polyvinylidene fluoride (PVDF; Aladdin Reagent Co., Ltd., Shanghai, China) and 7.5 g of PVA (Aladdin Reagent Co., Ltd., Shanghai, China) were dissolved in a mixed solvent consisting of 60 mL of dimethyl sulfoxide (DMSO; Sigma-Aldrich, USA) and 40 mL of reverse osmosis (RO) water. The solution was continuously stirred for 8 hours using a magnetic stirrer (Meiyingpu, China) in a controlled-temperature oil bath at 98°C (Smart, China), forming a uniform solution. The solution was then transferred into a test tube and placed in a freezer for 18 hours to solidify into a gel. Subsequently, the gel was thawed at 25°C for 6 hours to return to a liquid state. This freeze-thaw process was repeated three times, resulting in the formation of the PVA/PVDF hydrogel, which was sealed and stored for further use.

(2) Construction of AgNWs was as follows: to a 70 mL solution of ethylene glycol (China National Pharmaceutical Group Chemical Reagent Co., Ltd., China), PVP (K30) was added to form a 1.43% (w/v) PVP-ethylene glycol solution, which was then heated to 180°C to ensure complete dissolution of the PVP. Equal volumes and concentrations (45 µL each, 0.431 mol/L) of sodium chloride (China National Pharmaceutical Group Chemical Reagent Co., Ltd., China) and silver nitrate (Aladdin Reagent Co., Ltd., Shanghai, China) solutions were added dropwise to the PVP-ethylene glycol solution to form a silver chloride seed colloid. The mixture was then stirred for 5-10 minutes. Next, 25 mL of a 0.174 mol/L silver nitrate solution was slowly added to the reaction system, and stirring was stopped after 5 minutes of reaction. The reaction mixture was then subjected to repeated centrifugation and washed with ethanol to remove unreacted substances and impurities, yielding the AgNWs.

(3) Synthesis of nano-hydroxyapatite was as follows: a 100 mL solution of 11.80% (w/v) $Ca(NO_3)_2$ and a 6.58% (w/v) $(NH_4)_2HPO_4$ solution were mixed, and the pH was adjusted to 11 using ammonia solution. Then, 9.3 g of

ethylenediaminetetraacetic acid (EDTA; Nanjing Chemical Reagent Co., Ltd., China) was added. The mixture was placed in a forced-air constant-temperature drying oven (Shanghai Yiheng Scientific Instrument Co., Ltd., China) and underwent hydrothermal reaction at 180 °C for 6 hours. The nano-hydroxyapatite product was then retrieved.

(4) Fabrication of PVA/PVDF/AgNWs was as follows: 7.5 g of PVDF and 7.5 g of PVA were dissolved in a mixed solvent of 60 mL DMSO and 40 mL deionized water (DI water). The mixture was stirred at 98° C for 6 hours using a magnetic stirrer in an oil bath. The prepared AgNWs were then added, and the solution was stirred for an additional 2 hours. The mixture was subsequently placed in a freezer for 18 hours, followed by thawing at 25 ° C for 6 hours. This freeze-thaw process was repeated three times. The hydrogel was then immersed in ethanol at different concentrations in a 1:30 volume ratio for dehydration for at least 24 hours. The final PVA/PVDF/AgNWs piezoelectric composite hydrogel material was obtained.

(5) PVA/PVDF/AgNWs bilayer piezoelectric hydrogel was as follows: 7.5 g of PVDF and 7.5 g of PVA were dissolved in a mixed solvent consisting of 60 mL of DMSO and 40 mL of deionized water (DI water). To prepare the bone and cartilage layer solutions, 7 g of nano-hydroxyapatite and AgNWs were added, respectively. The bone layer solution was poured into a mold (2 mm thickness), and the cartilage layer solution (3 mm thickness) was quickly added on top to cover the bone layer. The mold was then placed in a freezer to freeze. The bilayer hydrogel was subsequently immersed in a 70% ethanol solution for 24 hours. Afterward, the hydrogel was removed and cut into 5 mm diameter samples using a 5 mm hole punch. The samples were washed, resulting in a bilayer PVA/PVDF/AgNWs piezoelectric hydrogel, with the cartilage layer on top and the bone layer on the bottom.

Hydrogel quality assessment

Characterization evaluation: (1) XRD characterization was performed on the prepared bilayer hydrogel. The hydrogel was sliced into thin films and dried. The X-ray diffractometer (STOE, Germany) was then activated, and the measurement parameters were set for XRD analysis. During the measurement, X-rays interacted with the crystalline structure of the sample, producing diffraction peaks. After the measurement, the obtained XRD patterns were analyzed.

(2) Fourier transform infrared spectroscopy (FTIR) characterization was implemented. Hydrogel samples were prepared as thin films and dried. FTIR analysis was performed using a FTIR spectrometer (PE Company, USA) with a scanning range of 400 cm^{-1} to 4,000 cm^{-1}, employing the attenuated total reflection (ATR) methodology. After scanning, the acquired infrared spectral data were transferred to a computer for further data processing and analysis.

(3) Microscopic characterization of the hydrogel morphology was performed as follows: First, the prepared hydrogel was subjected to freeze-drying. The dried hydrogel was then fractured, and the exposed surface was sputter-coated for surface morphology examination using scanning electron microscopy (SEM) (Thermo Fisher Scientific, USA).

Performance test: (1) Piezoelectric performance testing was conducted as follows: Hydrogel discs with a diameter of 10 mm and a thickness of 1 mm were initially prepared, and gold was sprayed onto both circular surfaces to create surface electrodes. Two wires were then fixed at both ends of the hydrogel disc as lead wires using conductive adhesive. The hydrogel material was encapsulated with an insulating polyurethane (PU) membrane to form a sealed package. A cyclic pressure test was conducted on the encapsulated hydrogel sample under a force of F = 15 N. A digital source measurement unit was used to monitor the piezoelectric performance of the hydrogel sample in real-time and collect data, recording voltage response data during the experiment. The piezoelectric performance of the hydrogel sample was evaluated based on the collected data.

(2) Hydrogel swelling performance testing was as follows. First, the hydrogel samples to be tested were prepared and pre-weighed, denoted as W, to ensure an accurate sample mass. Then, the hydrogel samples were placed into separate test tubes containing PBS with a pH of 7.4, ensuring consistent treatment conditions for each sample. The PBS buffer solution in the test tubes was placed on a shaker at 37°C to simulate physiological conditions. At different time points, the hydrogel samples were removed, and the solution on the sample surface was gently wiped away with filter paper to remove as much adhering liquid as possible, ensuring accurate mass data. The mass measurement of each sample was recorded as M_s, which is the sample mass after wiping away the surface solution at various time points. The swelling ratio Q of the hydrogel was calculated.

The changes in the Q value over time were recorded. These data were used for analyzing the swelling performance of the hydrogel samples, including the swelling rate and the final degree of swelling. Through this data, the dynamic swelling of the hydrogel at different time points can be assessed to understand its swelling behavior under physiological conditions.

(3) Mechanical performance was tested. Hydrogel tensile samples were prepared using standard molds with a dumbbell shape, with dimensions of 25 mm (length) × 2-3 mm (diameter) × 5 mm (width), ensuring that the sample dimensions met the requirements. The parameters for tensile testing were set on a universal tensile testing machine (Shimadzu Corporation, Japan), with a strain

rate of 5 mm/min set during the stretching process. The prepared tensile samples were placed in the testing fixtures, and the tensile test was initiated. During the test, the instrument gradually applied tensile force and recorded the stress-strain curve of the samples. Subsequently, hydrogel compression samples were prepared, shaped as cylinders with a diameter of 8 mm and a height of 3 mm. The prepared compression samples were placed in the testing fixtures, and compression testing was initiated.

***In vitro* cell experiment**

Fabrication of rabbit BMSCs: (1) Cell isolation was as follows. Rabbit BMSCs were purchased from Shanghai Fuyu Biotechnology Co., Ltd., China. The frozen BMSCs were first thawed in a 37°C constant temperature water bath. Subsequently, they were transferred to a 15 mL centrifuge tube and centrifuged at 1,200 rpm for 5 minutes. After centrifugation, the supernatant was discarded, and 3 mL of specialized rabbit BMSC culture medium was applied. The cells were then transferred to a culture flask and cultured in a 5% CO_2, 37°C cell culture incubator. The culture medium was changed every other day.

(2) Passaging was performed as follows: When the cell confluence in the culture flask reached 80-90%, 1 mL of trypsin digestion solution was added, and the cells were incubated in a 37° C incubator for 1-2 minutes to terminate the digestion. Next, 3 mL of fresh culture medium was added to prepare a cell suspension, followed by centrifugation at 1000 rpm for 5 minutes at 4° C. The cells were then resuspended in 2 mL of standard culture medium. The cells were passaged at a 1:3 dilution ratio and cultured in a sterile incubator at 37°C with 5% CO_2.

Cell intervention: Using 0.22 μm microporous filter membranes, lithium phenyl-2,4,6-trimethylbenzoylphosphate (LAP) solution (Shanghai Shenmin Industrial Co., Ltd., China), as well as the prepared solutions of PVA/PVDF hydrogel and PVA/PVDF/AgNWs hydrogel, were filtered to obtain corresponding sterile solutions. The BMSCs were grouped according to the intervention method, resulting in control group, PVA/PVDF group, and PVA/PVDF/AgNWs group. The 75 cm^2 cell culture flasks containing rabbit BMSCs were retrieved from the cell culture incubator. The culture medium appeared clear and bright with no signs of turbidity. When observing the flask inverted under a microscope, it was evident that the adherent cells had reached approximately 90% confluence. The cells were digested for 1-2 minutes at 37°C in the cell culture incubator. After centrifugation and removal of the supernatant, each tube was supplemented with 5 mL of the respective sterile solutions mentioned earlier (physiological saline for the control group). The cells were thoroughly mixed with the materials to obtain a cell suspension containing the materials. Cell counting was performed using a cell counter to ensure a cell concentration of 10^6 cells/mL. Subsequently, 50 μL of LAP solution was added gently while avoiding exposure to light. A 100 mL cell suspension solution was aspirated and added to mold wells. It was exposed to 365 nm ultraviolet light for 1 minute. This process resulted in the encapsulation of cells within the hydrogel. Subsequently, the hydrogel-cell composite was transferred to a 48-well plate, with one composite in each well. Each well was supplemented with 1 mL of regular culture medium, and the wells were labeled according to their corresponding groups. The 48-well plate was then placed in a cell culture incubator at 37°C in a sterile environment with 5% CO_2 and humidity. After two days of incubation, the culture medium was changed.

Detection of cell survival: The reagents from the Calcein-AM/PI Double Stain Kit (Biogradetech, USA) were placed in a laminar flow hood, and a 10-fold dilution with PBS was performed to obtain 1× Assay Buffer. Subsequently, a working solution was prepared by mixing 5 μL of Calcein-AM solution (2 mM) and 15 μL of PI solution (1.5 mM) with 5 mL of 1× Assay Buffer, ensuring thorough mixing. After 3 days of cultivation, the 48-well plates from each group were removed from the cell culture incubator. Three random samples were selected from each group. The culture medium was removed, and the cells were washed three times with PBS solution. Subsequently, 500 μL of Calcein-AM/PI working solution was added to each well, and the plates were incubated at 37° C for 30 minutes. After incubation, the Calcein-AM/PI working solution was removed, and the cells were washed three times with PBS solution. Next, 500 μL of regular culture medium was applied to each well, and the cells were observed and photographed under a fluorescence microscope. Dead cells were stained red, while live cells were stained green (KEYENCE, Japan). Cell counting and the calculation of the proportion of live cells were performed using *ImageJ*.

Western blotting: Total cellular proteins were extracted using RIPA lysis buffer and quantified via BCA assay. Proteins (30 μg per lane) were separated by 10% SDS-PAGE and electrophoretically transferred onto PVDF membranes. After blocking with 5% non-fat milk for 2 h at room temperature, membranes were incubated overnight at 4° C with primary antibodies: anti-COL2A1 (1:2000), anti-ACAN (1:2000), anti-SOX9 (1:2000), and anti-GAPDH (1:1000) as loading control. Following three TBST washes (5 min each), membranes were probed with HRP-conjugated secondary antibodies (1:8000) for 1 h at room temperature. Protein bands were visualized using enhanced chemiluminescence and quantified by densitometry with ImageJ software.

Animals experiment

Animals grouping and model establishment: Thirty healthy adult female New Zealand white rabbits (6 to 8 months old, body weight 2.5 to 3.0 kg) were obtained from Shandong Qinbo Breeding Co., Ltd., China. The rabbits were housed under standard conditions (25° C) and provided with adequate food and water. All experiments were approved by Ethics Committee of Hospital, and in accordance with the Guide for the Care and Use of Laboratory Animals published by the United States National Institutes of Health. The rabbits were randomly assigned into Group A (control group without any intervention, blank control), Group B (intervention treatment with PVA/PVDF hydrogel) and Group C (intervention treatment with PVA/PVDF/AgNWs hydrogel), each group with 10 rabbits.

The ears of the rabbits were wiped with anhydrous ethanol to expose the marginal ear vein. Subsequently, 5 mL of 10% (w/v) pentobarbital sodium (MackLin Biotech Co., Ltd., China) was injected into the rabbits for anesthesia. The right knee joint area of the rabbits was shaved, and an incision was made to access the joint cavity, providing a pathway for subsequent surgery. Next, a 5 mm diameter hole was drilled at the distal femoral trochlea of the rabbit's knee joint, penetrating the bone marrow cavity to a depth of approximately 4-5 mm, simulating the cartilage defect. The wound was cleaned with gauze and physiological saline, and the experimental hydrogel was implanted into the cartilage defect. The femur was then repositioned to its normal location, and the muscles and skin around the knee joint were sutured to close the surgical incision. Postoperatively, one million units of penicillin were administered for three consecutive days to prevent bacterial infection and alleviate postoperative discomfort in the rabbits. The rabbits' mental and physiological status was continuously monitored to ensure their recovery and well-being.

General observation of cartilage repair: At eight weeks post-surgery, rabbits were euthanized using the air embolism methodology. The articular cartilage was extracted from the rabbits, and photographs were taken using a digital camera to document and assess the repair status, smoothness, and size differences relative to the surrounding tissues at the defect site. Evaluation was performed using the *International Cartilage Repair Society* (ICRS) scoring criteria. The specimens were then placed in a 10% formaldehyde solution for fixation. The specimens were soaked in formaldehyde for three days to ensure adequate tissue fixation. After fixation in a 4% phosphate-buffered formalin solution for 48 hours, the specimens were placed in a Micro-CT system (Yinxi Biotechnology Co., Ltd., China) and subjected to evenly spaced thin-section scans of the femoral specimens under the following conditions: 45 kV, 250.0 μA current, 245.0 ms exposure time, and a slice thickness of 0.1 mm.

Histological observation of cartilage repair: At eight weeks post-surgery, all remaining rabbits, except those mentioned above, were euthanized using the air embolism method. The articular cartilage was extracted and fixed in a 10% formaldehyde solution for three days, then decalcified in a 10% Ethylene Diamine Tetraacetic Acid solution (Sigma-Aldrich, USA) for 14 days with daily solution changes. The tissue was dehydrated through a graded ethanol series (70%-100%), embedded in paraffin, sectioned at a thickness of 5 μm using a rotary microtome (Leica RM2235, Germany). The sections were stained with a hematoxylin and eosin (H&E) staining kit (Beyotime Biotechnology Co., Ltd., China) according to the manufacturer's protocol: hematoxylin incubation (5 minutes), eosin counterstaining (2 minutes), and ethanol dehydration. Two pathologists, blinded to the experimental conditions, assessed the histomorphology using the Schreiner scoring system (Schreiner *et al*. 2021). The evaluation parameters included: tissue structure (0-4 points), chondrocyte density (0-3 points), cartilage-bone integration (0-3 points), and degree of calcification (0-2 points).

Statistical analysis: All experimental data were statistically analyzed using *SPSS 19.0*, and the data were presented as means ± standard deviations. Differences between two independent sample groups were assessed using Student's t-test, while differences among multiple groups were assessed using one-way analysis of variance (ANOVA). A significance level of $P<0.05$ was defined to indicate statistical significance.

RESULTS

Characterization results of PVA/PVDF/AgNWs piezoelectric composite double-layer hydrogel: For XRD characterization of the materials, this study conducted a comparative analysis to investigate the changes before and after the addition of AgNWs. Upon the addition of AgNWs, there was a significant enhancement in the peak intensity at 21.38° corresponding to the piezoelectric β-phase of the material compared to the case without AgNWs (Figure 1A). Based on the FTIR analysis, it was concluded that the spectral comparison between samples with and without AgNWs did not show significant changes. However, a comparison of the characteristic peaks of the PVDF β-phase before and after the addition of AgNWs revealed an enhancement in the peak intensity at 902 cm^{-1} for different ratios of added AgNWs (Figure 1B). The SEM image of the PVA/PVDF/AgNWs hydrogel network reveals a distinct three-dimensional porous structure internally, with pore diameters approximately ranging from 40-50 μm (Figure 1C). The surface elemental

mapping of the incorporated AgNWs and nano-hydroxyapatite, demonstrating their uniform distribution within the hydrogel structure (Figure 1 D-E).

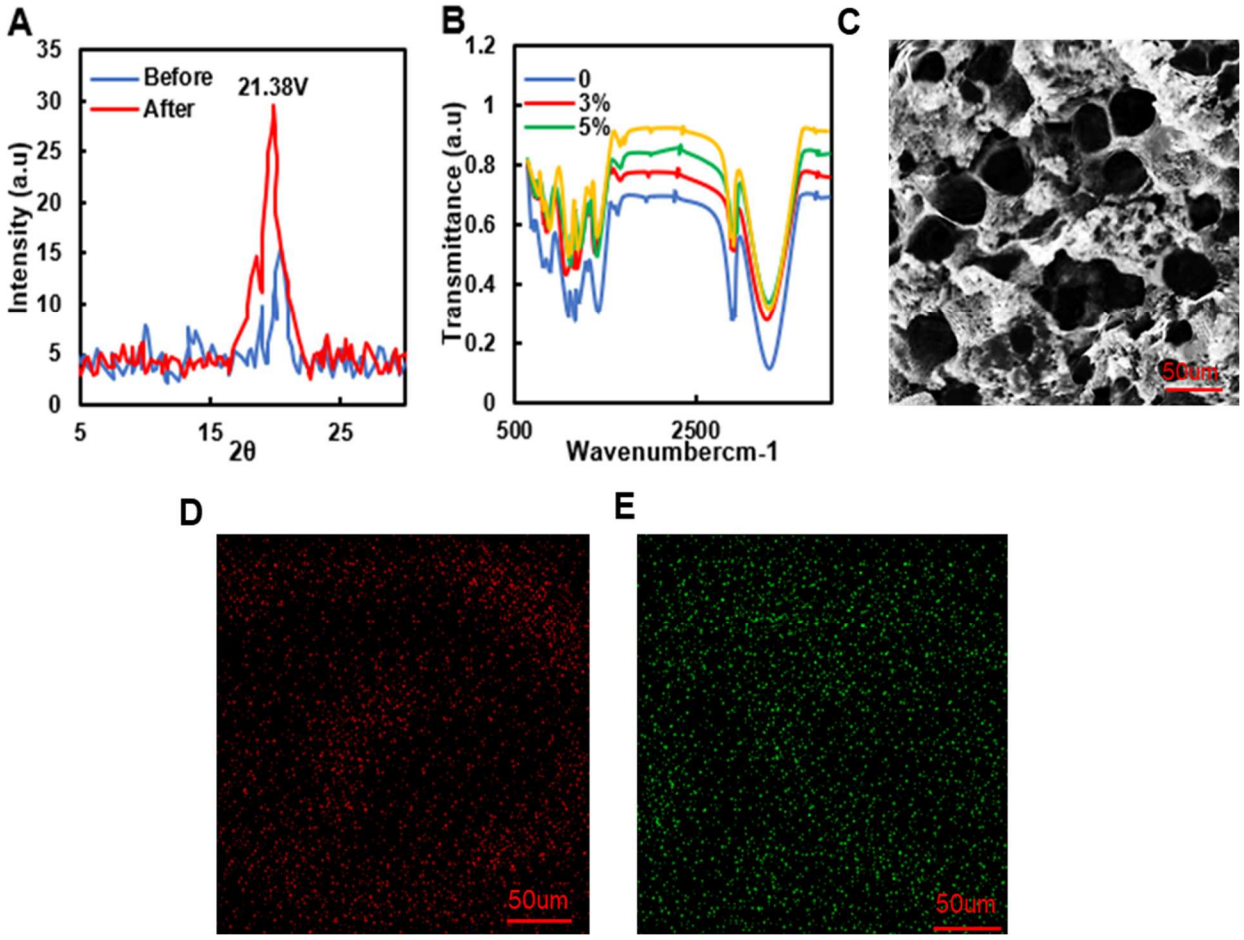

Figure 1. Hydrogel characterization analysis results. A: XRD characterization analysis; B: FTIR; C: SEM observation; D: AgNWs distribution image; E: HA distribution image.

Performance results of PVA/PVDF/AgNWs piezoelectric composite double-layer hydrogel: For different proportions of AgNWs, the piezoelectric voltage fluctuated from 0.29 V to 0.39 V, showing no significant impact on the piezoelectric performance of the gel (Figure 2A-C). Based on these results, this study selected 0.3% AgNWs as the standard proportion for subsequent experiments. The piezoelectric hydrogel reached a relatively stable state after swelling for approximately 6 hours under different ethanol concentration gradients. With the ethanol concentration increased, the swelling ratio of the piezoelectric hydrogel increased from about 15-fold to approximately 60-fold (Figure 2D). The compressive performance of the hydrogel at different ethanol concentrations exhibited nonlinear viscoelastic behavior, with the compressive modulus increasing with higher ethanol concentrations (Figure 3A). Additionally, the stress-strain curves of the hydrogel exhibited an increasing trend under tension (Figure 3B). With increasing ethanol concentration, the tensile fracture strength increased from 0.26 MPa to approximately 0.6 MPa.

In vitro experimental results

Cell survival test results: Staining of the cells within the hydrogel was performed using the Calcein-AM/PI Double Stain Kit, where green fluorescence indicates live cells, and red fluorescence indicates dead cells. The results revealed that there were fewer dead cells in the Control group, the PVA/PVDF group, and the PVA/PVDF/AgNWs group, indicating that the hydrogel did not exhibit significant cytotoxicity (Figure 4A). Furthermore, analysis using *Image J* showed neglectable differences in the proportion of live cells between the PVA/PVDF group and PVA/PVDF/AgNWs group when compared to control group (P>0.05), with all groups having a live cell proportion exceeding 85% (Figure 4B).

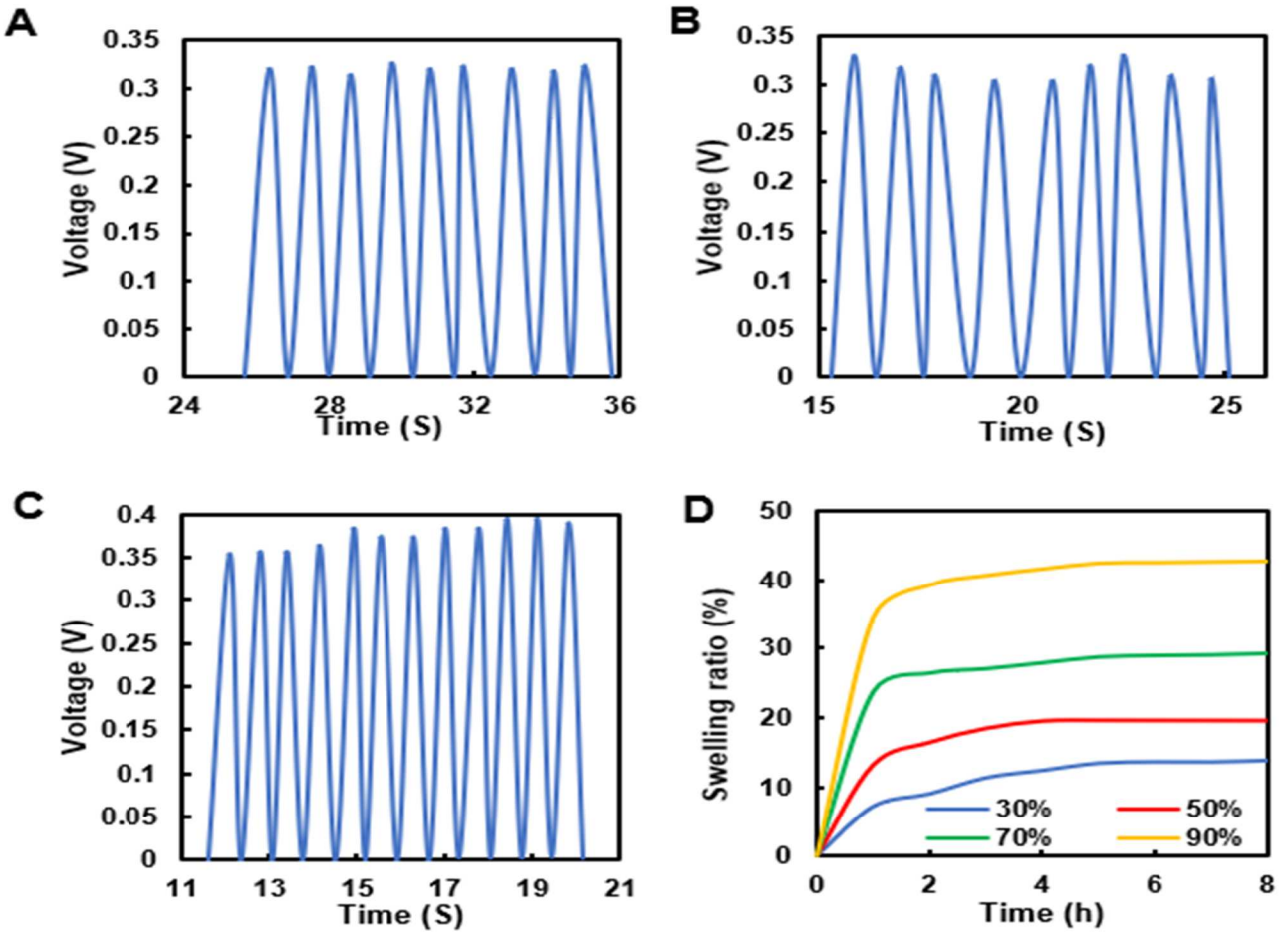

Figure 2. Test results of piezoelectric and swelling properties. A: piezoelectric properties of 0.3% AgNWs; B: piezoelectric properties of 0.5% AgNWs; C: piezoelectric properties of 0.7% AgNWs; D: swelling behavior under different ethanol concentrations.

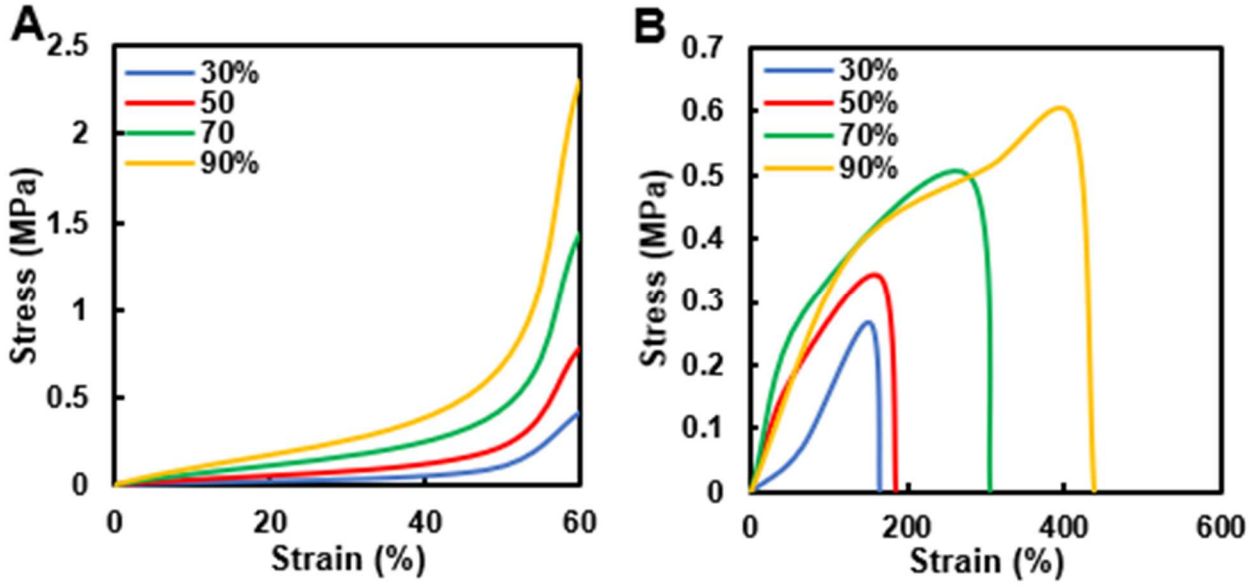

Figure 3. Mechanical performance test results. A: compression performance; B: tensile properties.

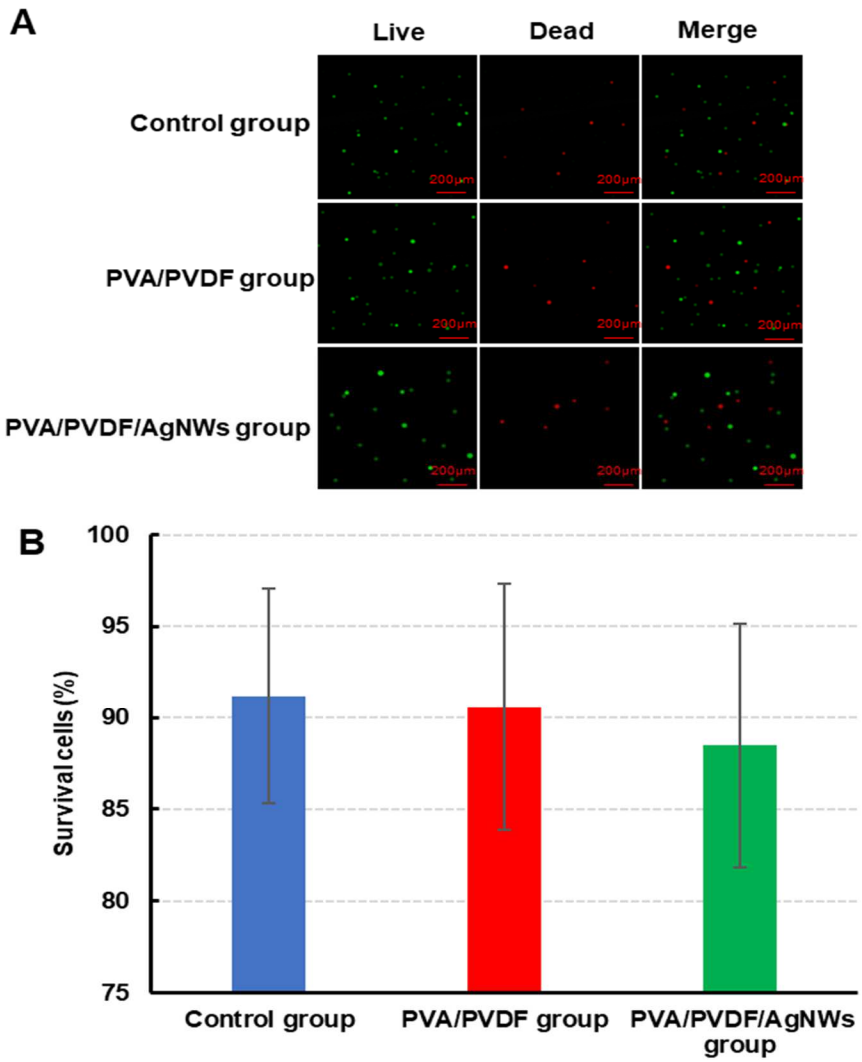

Figure 4. Cell state detection results. A: live/dead staining result chart; B: live cell ratio.

Cartilage biomarker content detection results: Compared to the Control group, the protein expression levels of COL2A1, ACAN, and SOX9 in the PVA/PVDF group and PVA/PVDF/AgNWs group were significantly increased ($P < 0.05$), and the protein expression levels of COL2A1, ACAN, and SOX9 in the PVA/PVDF/AgNWs group were higher than those in the PVA/PVDF group ($P < 0.05$) (Figure 5).

Animal experiment results

General observation results of articular cartilage in rabbits: Group A exhibited evident tissue defects in rabbit joint cartilage, while Group B showed partial neocartilage tissue formation at the implant site but still presented some residual defects. In contrast, Group C exhibited nearly complete coverage of neocartilage at the defect site, which appeared smoother and tightly connected to the surrounding tissue. The ICRS scoring results also demonstrated that the ICRS score of Group C was significantly higher than that of the Group A and Group B ($P<0.05$), with Group A having the lowest score (Figure 6).

Histological observation results of rabbit articular cartilage: The histological analysis results revealed distinct outcomes among the different groups. In Group A, characterized by the absence of any treatment or repair materials, evident tissue damage was observed. In Group B, the defect area showed some generation of subchondral bone and chondrocytes, although the degree of integration of these cells was not pronounced. In contrast, Group C exhibited notably improved results, with substantial repair of both bone and cartilage at the defect site. This group demonstrated the presence of a normal and intact bone-cartilage physiological structure, with a close and indistinct interface boundary. Histological scoring results also indicated that Group C's repair outcome was substantially superior to the Group A and Group B ($P<0.05$) (Figure 7).

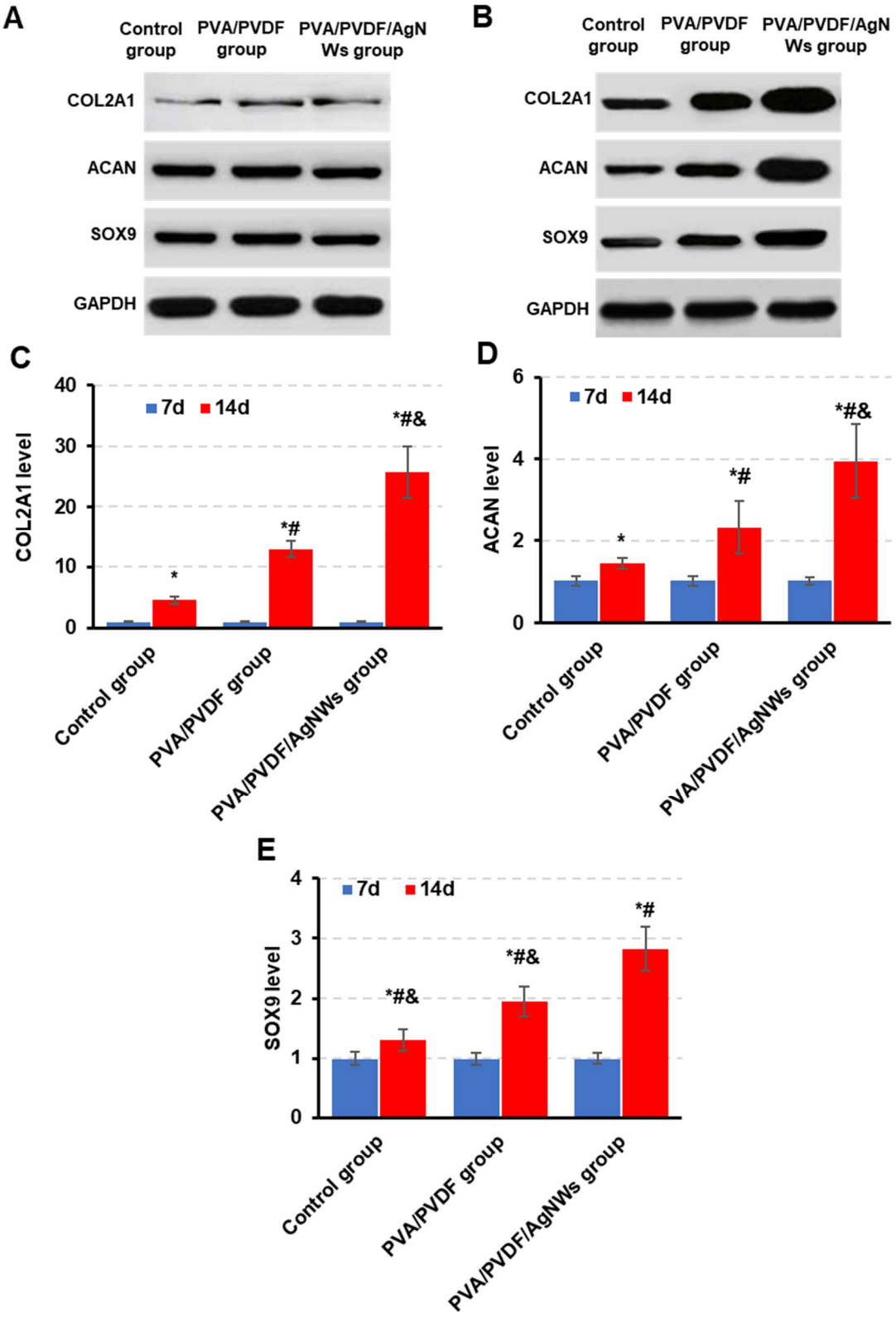

Figure 5. Detection of cartilage biomarker content. A: Western blot analysis of proteins at day 7 of culture; B: Western blot analysis of proteins at day 14 of culture; C: COL2A1 protein expression level; D: ACAN protein expression level; E: SOX9 protein expression level. **P*<0.05 vs. 7 days; #*P*<0.05 vs. control group; &*P*<0.05 vs. PVA/PVDF group.

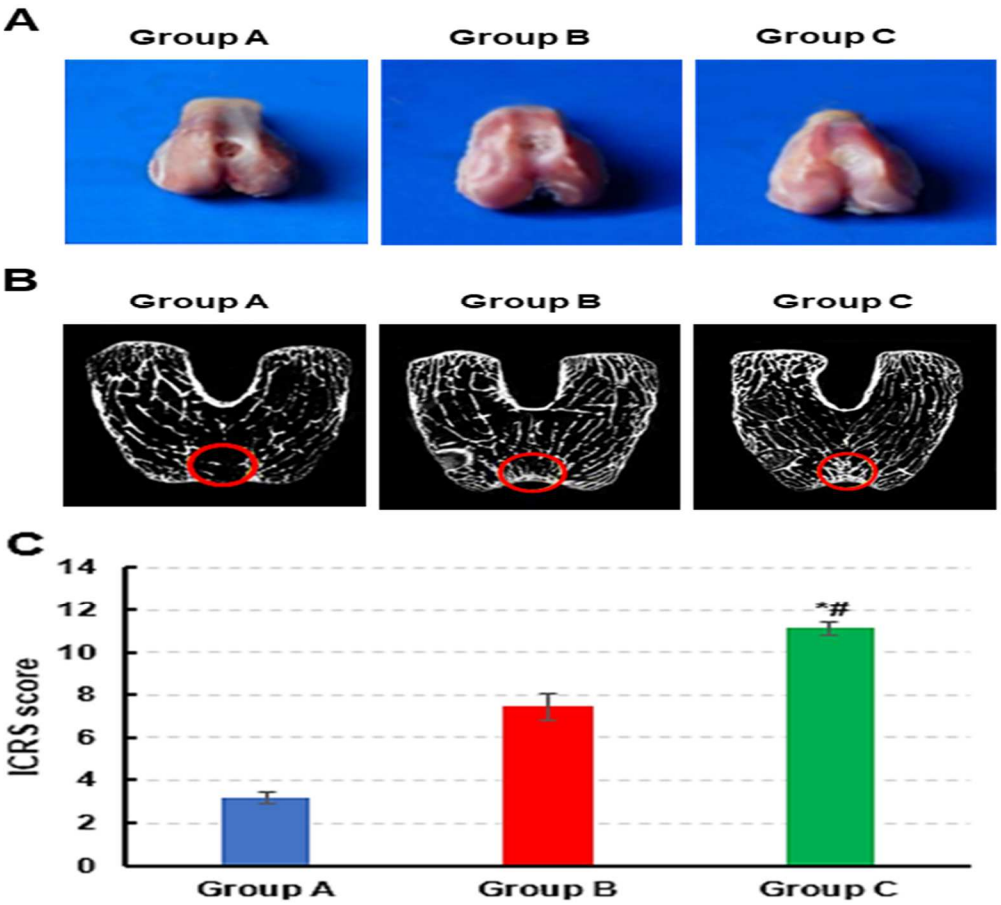

Figure 6. General observation results of joint cartilage repair. A: bare bone samples; B: micro-CT 3D reconstruction image, with red circles representing the defect area; C: ICRS score; **P*<0.05 vs. Group A; #*P*<0.05 vs. Group B.

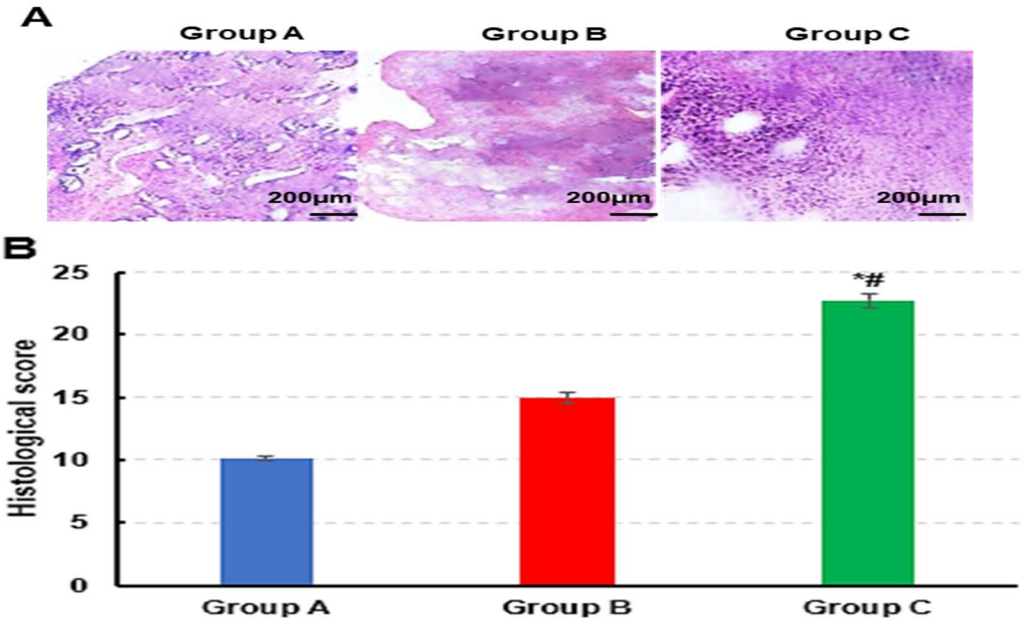

Figure 7. Histological observation results of articular cartilage repair. A: HE staining sample; B: organizational scoring; **P*<0.05 vs. Group A; #*P*<0.05 vs. Group B.

DISCUSSION

Bone deficiency resulting from trauma or surgery is termed bone defects. Bone defects can lead to non-union, delayed healing, or non-healing, causing local functional impairments. The primary treatment approach for bone defects is bone grafting, such as autologous cancellous bone transplantation. Advances in microsurgical techniques, bone external fixation methods, biomaterials, and bone tissue engineering have contributed to significant progress in clinical treatment of bone defects. In this study, PVA/PVDF/AgNWs composite materials were prepared and characterized. XRD analysis showed no significant change in the piezoelectric β-phase characteristic peak of the composite material before and after the addition of nanosilver. This indicates that the inclusion of nanosilver enhances the crystallinity of β-phase in PVDF, thereby improving the material's piezoelectric performance (Guo *et al*. 2019). The β-phase is the main crystal phase affecting the piezoelectric properties of PVDF, thus enhancing the material's piezoelectric performance. This result may be attributed to nanosilver acting as a crystal nucleus in the material, promoting the growth of β-phase crystals and thereby enhancing the material's piezoelectric performance. Subsequent morphological observations of the PVA/PVDF/AgNWs composite material revealed a three-dimensional mesh pore structure, with nanosilver and nano-hydroxyapatite uniformly distributed within the gel. This indicates that the addition of nanosilver wires facilitates the formation of more β-phase crystallization in PVDF during the molding process, thereby improving the material's performance (He *et al*. 2021). The phase separation structure between PVA and PVDF results in PVDF being uniformly distributed on the PVA network structure or filled inside the pores, effectively enhancing the material's toughness and promoting the formation of PVDF β-phase and improving the osteogenic performance of the material. Furthermore, this study found that adding different concentrations of ethanol to the PVA/PVDF/AgNWs composite material affects its water absorption properties. Specifically, the higher the ethanol concentration, the more pronounced the volume contraction of the hydrogel during dehydration. This is because high-concentration ethanol has lower surface tension and higher volatility, which makes it easier for water molecules inside the hydrogel to be displaced during dehydration. In the subsequent water absorption process, the hydrogel that has undergone significant volume contraction forms more pores internally, thereby exhibiting stronger water absorption capacity (Sabzi *et al*. 2020). Lastly, this study discovered that the tensile strength of the PVA/PVDF/AgNWs composite material increases with increasing ethanol concentration. These experimental results demonstrated the significant impact of factors such as nanosilver content and ethanol concentration on the performance of piezoelectric hydrogels, providing valuable information for designing and controlling hydrogel properties. These performance characteristics make piezoelectric hydrogels a potential biomedical material suitable for applications such as articular cartilage repair (Pan *et al*. 2021).

This study assessed the cytotoxicity of PVA/PVDF/AgNWs composite materials and found that the cell viability after co-culture with cells was >85%. This result further confirms the excellent biocompatibility of all hydrogel groups, indicating no cytotoxicity was induced. COL2A1 encodes type II collagen, a major structural protein in cartilage tissue that forms the collagen fiber network, imparting cartilage with its unique elasticity and toughness (Zhang *et al*. 2020). ACAN encodes aggrecan, which occupies most of the cartilage matrix, possessing high negativity to maintain cartilage hydration and resistance to compression (Lin *et al*. 2021). SOX9 is a key transcription factor that regulates chondrocyte differentiation and maturation during embryonic development. SOX9 regulates mesenchymal stem cell chondrogenic differentiation and maintains the chondrocytic phenotype (Song *et al*. 2020). This study found that after co-culturing PVA/PVDF/AgNWs composite materials with BMSCs, the expression levels of COL2A1, ACAN, and SOX significantly increased. Increased expression of COL2A1, ACAN, and SOX indicates ongoing cell differentiation and proliferation in cartilage tissue, which are typical physiological responses during cartilage repair and regeneration (Liu *et al*. 2021). This study found that after implanting PVA/PVDF/AgNWs composite materials into rabbit articular cartilage, there was a significant increase in the overall ICRS score, and histological examination (HE staining) revealed a more intact physiological structure at the defect site with tight interface integration. The ICRS score is a standardized method for evaluating the effectiveness of articular cartilage repair (Schagemann *et al*. 2022). These research findings demonstrate that PVA/PVDF/AgNWs piezoelectric composite bilayer hydrogels play a significant role in promoting cartilage repair, notably enhancing chondrocyte proliferation and cartilage tissue regeneration, thereby facilitating more effective defect repair. The piezoelectric properties of the hydrogel may provide additional mechanical stimulation for tissue growth and repair, facilitating cartilage formation (Zhou *et al*. 2023)]. Therefore, these findings hold promise for significant breakthroughs in clinical applications and tissue engineering research.

Conclusion: This study successfully fabricated a PVA/PVDF/AgNWs composite bilayer nanohydrogel, which exhibits low biotoxicity and promotes the expression of rabbit chondrocyte markers, facilitating cartilage tissue growth and repair. However, further

large-scale and long-term studies are required to validate its long-term efficacy and stability. In conclusion, this research provides a novel approach for cartilage defect repair.

Acknowledgment: None.

Author's contribution: Conception and study design: Xuan Sun, Shuai Wang and Feng Ji; data acquisition and analysis: Shuai Wang, Honghui Tang and Haitao Yue; manuscript draft, editing and revision: Xuan Sun, Shuai Wang and Feng Ji. All authors wrote and approved the final manuscript.

Animal Ethics: All experiments were approved by Ethics Committee of The Affiliated Huai'an No.1 People's Hospital of Nanjing Medical University (Huai'an, China), and in accordance with the Guide for the Care and Use of Laboratory Animals published by the United States National Institutes of Health.

Funding: None.

REFERENCES

Abdollahiyan, P., F. Oroojalian, A. Mokhtarzadeh, and M. de la Guardia. (2020). Hydrogel - Based 3D Bioprinting for Bone and Cartilage Tissue Engineering. Biotechnol J. 15(12): e2000095. https://doi.org/10.1002/biot.202000095

Ahmadi, N., M. Kharaziha, and S. Labbaf. (2019). Core - shell fibrous membranes of PVDF - Ba0.9Ca0.1TiO3/PVA with osteogenic and piezoelectric properties for bone regeneration. Biomater (Bristol, England). 15(1):015007. https://doi.org/10.1088/1748 - 605X/ab5509

Anastasio, A.T., A. Chopra, N.M. Madi, T.Q. Tabarestani, A.N. Fletcher, S.G. Parekh. (2024). Polyvinyl Alcohol Hydrogel Hemiarthroplasty of First Metatarsophalangeal Joint Hallux Rigidus. Cureus. 16(4):e58583. https://doi.org/10.7759/cureus.58583

Bai, Y., Y. Liu, H. Lv, H. Shi, W. Zhou, Y. Liu, and D.G. Yu. (2022). Processes of Electrospun Polyvinylidene Fluoride - Based Nanofibers, Their Piezoelectric Properties, and Several Fantastic Applications. Polymers. 14(20):4311. https://doi.org/10.3390/polym14204311

Benmassaoud, M.M., K.A. Gultian, M. DiCerbo, and S.L. Vega. (2020). Hydrogel screening approaches for bone and cartilage tissue regeneration. Ann N Y Acad Sci. 1460(1):25 – 42. https://doi.org/10.1111/nyas.14247

Campos, Y., A. Almirall, G. Fuentes, H.L. Bloem, E.L. Kaijzel, and L.J. Cruz. (2019). Tissue Engineering: An Alternative to Repair Cartilage. Tissue Eng Part B Rev. 25(4):357 - 373. https://doi.org/10.1089/ten.TEB.2018.0330

Cooper, S.M., and R.S. Rainbow. (2022). The Developing Field of Scaffold - Free Tissue Engineering for Articular Cartilage Repair. Tissue Eng Part B Rev. 28(5):995 - 1006. https://doi.org/10.1089/ten.TEB.2021.0130

Guo, Y., S. Wang, H. Du, X. Chen, and H. Fei. (2019). Silver Ion - Histidine Interplay Switches Peptide Hydrogel from Antiparallel to Parallel β - Assembly and Enables Controlled Antibacterial Activity. Biomacromolecules. 20(1):558 – 565. https://doi.org/10.1021/acs.biomac.8b01480

He, Z., F. Rault, M. Lewandowski, E. Mohsenzadeh, and F. Salaün. (2021). Electrospun PVDF Nanofibers for Piezoelectric Applications: A Review of the Influence of Electrospinning Parameters on the β Phase and Crystallinity Enhancement. Polymers. 13(2):174. https://doi.org/10.3390/polym13020174

Jabeen, N., A. Roy, R. Senthil. (2024). Evaluation and In Vitro Study of an Electrospun Bone Tissue Membrane for Bone Regeneration: A Novel Perspective. Cureus. 16(1):e52830. https://doi.org/10.7759/cureus.52830

Khajeh, S., F. Bozorg - Ghalati, M. Zare, G. Panahi, and V. Razban. (2021). Cartilage Tissue and Therapeutic Strategies for Cartilage Repair. Curr Mol Med. 21(1):56 - 72. https://doi.org/10.2174/1566524020666620061017 0646

Li, D.S., Z. Pan, C.C. Cai, T.T. Li, C.W. Lou, J.H. Lin, and H.T. Ren (2023). Synergy of Adsorption and Photocatalytic Reduction for Efficient Removal of Cr(VI) with Polyvinylidene Fluoride@Polyvinyl Alcohol - FeC2O4/Bi2.15WO6. Langmuir. 39(30):10601 – 10610. https://doi.org/10.1021/acs.langmuir.3c01203

Li, Y., C. Liao, and S.C. Tjong. (2019). Electrospun Polyvinylidene Fluoride - Based Fibrous Scaffolds with Piezoelectric Characteristics for Bone and Neural Tissue Engineering. Nanomaterials (Basel). 9(7):952. https://doi.org/10.3390/nano9070952

Lin, L., M. Li, J. Luo, P. Li, S. Zhou, Y. Yang, K. Chen, Y. Weng, X. Ge, M. Mireguli, H. Wei, H. Yang, G. Li, Y. Sun, L. Cui, S. Zhang, J. Chen, G. Zeng, L. Xu, X. Luo, and Shen Y (2021) A High Proportion of Novel ACAN Mutations and Their Prevalence in a Large Cohort of Chinese Short Stature Children. J Clin Endocrinol Metab. 106(7):e2711 – e2719. https://doi.org/10.1210/clinem/dgab088

Liu, H., Y. Rui, J. Liu, F. Gao, and Y. Jin. (2021). Hyaluronic acid hydrogel encapsulated BMP - 14 - modified ADSCs accelerate cartilage defect repair in rabbits. J Orthop Surg Res. 16(1):657. https://doi.org/10.1186/s13018-021-02792-w

Pan, Y., P. Li, F. Liang, J. Zhang, J. Yuan, and M. Yin. (2021). A Nano - Silver Loaded PVA/Keratin Hydrogel With Strong Mechanical Properties Provides Excellent Antibacterial Effect for Delayed Sternal Closure. Front Bioeng Biotechnol. 9:733980. https://doi.org/10.3389/fbioe.2021.733980

Pour, G.B., L.F. Aval, and M. Mirzaee. (2020). CNTs Supercapacitor Based on the PVDF/PVA Gel Electrolytes. Recent Pat Nanotechnol. 14(2):163-170. https://doi.org/10.2174/1872210513666191204111006

Sabzi, M., M.J. Afshari, M. Babaahmadi, and N. Shafagh. (2020). pH - dependent swelling and antibiotic release from citric acid crosslinked poly(vinyl alcohol) (PVA)/nano silver hydrogels. Colloids Surf B Biointerfaces. 188:110757. https://doi.org/10.1016/j.colsurfb.2019.110757

Sakarkar, S., S. Muthukumaran, and V. Jegatheesan. (2020). Evaluation of polyvinyl alcohol (PVA) loading in the PVA/titanium dioxide (TiO2) thin film coating on polyvinylidene fluoride (PVDF) membrane for the removal of textile dyes. Chemosphere. 257:127144. https://doi.org/10.1016/j.chemosphere.2020.127144

SantAnna, J.P.C., R.R. Faria, I.P. Assad, C.C.G. Pinheiro, V.D. Aiello, C. Albuquerque - Neto, R. Bortolussi, I.A. Cestari, M.J.S. Maizato, A.J. Hernandez, D.F. Bueno, and T.L. Fernandes. (2022) Tissue Engineering and Cell Therapy for Cartilage Repair: Preclinical Evaluation Methods. Tissue Eng Part C Methods. 28(2):73 – 82. https://doi.org/10.1089/ten.TEC.2021.0208

Schagemann, J.C., L. Galle, J. Gille, A. Frydrychowicz, G. Welsch, G. Salzmann, A. Paech, and H. Mittelstaedt. (2022). Correlation of the Histological ICRS II Score and the 3D MOCART Score for the Analysis of Aged Osteochondral Regenerates in a Large Animal Model. Cartilage. 13(1):19476035211072254. https://doi.org/10.1177/19476035211072254

Schreiner, M.M., M. Raudner, S. Marlovits, K. Bohndorf, M. Weber, M. Zalaudek, S. Röhrich, P. Szomolanyi, G. Filardo, R. Windhager, and S. Trattnig. (2021). The MOCART (Magnetic Resonance Observation of Cartilage Repair Tissue) 2.0 Knee Score and Atlas. Cartilage. 13(1_suppl):571S-587S. https://doi.org/10.1177/1947603519865308

Shen, K., A. Duan, J. Cheng, T. Yuan, J. Zhou, H. Song, Z. Chen, B. Wan, J. Liu, X. Zhang, Y. Zhang, R. Xie, F. Liu, W. Fan, and Q. Zuo. (2022). Exosomes derived from hypoxia preconditioned mesenchymal stem cells laden in a silk hydrogel promote cartilage regeneration via the miR - 205 - 5p/PTEN/AKT pathway. Acta Biomater. 143:173 – 188. https://doi.org/10.1016/j.actbio.2022.02.026

Song, H., and K.H. Park. (2020). Regulation and function of SOX9 during cartilage development and regeneration. Semin Cancer Biol. 67(Pt 1):12 – 23. https://doi.org/10.1016/j.semcancer.2020.04.008

Torres – Rodriguez, J., D. Bedolla, F. D'Amico, A.K. Koopmann, L. Vaccari, G. Saccomano, R. Kohns, and N. Huesing. (2022). Polyvinylidene Fluoride Aerogels with Tailorable Crystalline Phase Composition. Gels (Basel, Switzerland). 8(11):727. https://doi.org/10.3390/gels8110727

Vishwakarma, V., J. Kandasamy, and S. Vigneswaran. (2023). Surface Treatment of Polymer Membranes for Effective Biofouling Control. Membranes. 13(8):736. https://doi.org/10.3390/membranes13080736

Wang, L., Y. Yu, X. Zhao, Z. Zhang, X. Yuan, J. Cao, W. Meng, L. Ye, W. Lin, and G. Wang. (2022). A Biocompatible Self - Powered Piezoelectric Poly(vinyl alcohol) - Based Hydrogel for Diabetic Wound Repair. ACS Appl Mater Interfaces. 14(41):46273 – 46289. https://doi.org/10.1021/acsami.2c13026

Wang, W., Y. Shi, G. Lin, B. Tang, X. Li, J. Zhang, X. Ding, and G. Zhou. (2023). Advances in Mechanical Properties of Hydrogels for Cartilage Tissue Defect Repair. Macromol Biosci. 23(7):e2200539. https://doi.org/10.1002/mabi.202200539

Yu, Y., Y. Yang, L. Yu, K.Y. Koh, and J.P. Chen. (2021). Modification of polyvinylidene fluoride membrane by silver nanoparticles - graphene oxide hybrid nanosheet for effective membrane biofouling mitigation. Chemosphere. 268:129187. https://doi.org/10.1016/j.chemosphere.2020.129187

Zhang, B., Y. Zhang, N. Wu, J. Li, H. Liu, and J. Wang. (2020). Integrated analysis of COL2A1 variant data and classification of type II collagenopathies. Clin Genet. 97(3):383 – 395. https://doi.org/10.1111/cge.13680

Zhang, F.X., P. Liu, W. Ding, Q.B. Meng, D.H. Su, Q.C. Zhang, R.X. Lian, B.Q. Yu, M.D. Zhao, J.

Dong, Y.L. Li, and L.B. Jiang. (2021). Injectable Mussel - Inspired highly adhesive hydrogel with exosomes for endogenous cell recruitment and cartilage defect regeneration. Biomaterials 278:121169. https://doi.org/10.1016/j.biomaterials.2021.121169

Zhao, H., J. Huang, Y. Li, X. Lv, H. Zhou, H. Wang, Y. Xu, C. Wang, J. Wang, and Z. Liu. (2020). ROS - scavenging hydrogel to promote healing of bacteria infected diabetic wounds. Biomaterials 258:120286. https://doi.org/10.1016/j.biomaterials.2020.120286

Zhao, Y., Z. Cui, B. Liu, J. Xiang, D. Qiu, Y. Tian, X. Qu, and Z. Yang. (2019). An Injectable Strong Hydrogel for Bone Reconstruction. Adv Healthcare Mater. 8(17):e1900709. https://doi.org/10.1002/adhm.201900709

Zhou, Z., J. Zheng, X. Meng, and F. Wang. (2023). Effects of Electrical Stimulation on Articular Cartilage Regeneration with a Focus on Piezoelectric Biomaterials for Articular Cartilage Tissue Repair and Engineering. Int J Mol Sci. 24(3):1836. https://doi.org/10.3390/ijms24031836

Zhu, J., S. Yang, Y. Qi, Z. Gong, H. Zhang, K. Liang, P. Shen, Y.Y. Huang, Z. Zhang, W. Ye, L. Yue, S. Fan, S. Shen, A.G. Mikos, X. Wang, and X. Fang. (2022). Stem cell - homing hydrogel - based miR - 29b - 5p delivery promotes cartilage regeneration by suppressing senescence in an osteoarthritis rat model. Sci Adv. 8(13):eabk0011. https://doi.org/10.1126/sciadv.abk0011.